Meteorol. Z. (Contrib. Atm. Sci.)
Published online August 2024

Open Access Early Access Article
Boundary Layer Meteorology

High-resolution ensemble LES energy balance closure study of the LITFASS-2003 campaign

Sadiq Huq[1], Frederik De Roo[1,4], Matthias Sühring[3,6], Luise Wanner[1,2], Matthias Mauder[1,2,5,*]

[1] Institute of Meteorology and Climate Research, Atmospheric Environmental Research (IMK-IFU), Karlsruhe Institute of Technology (KIT), Garmisch-Partenkirchen, Germany
[2] Institute of Hydrology and Meteorology, TUD Dresden University of Technology, Tharandt, Germany
[3] Institute of Meteorology and Climatology, Leibniz University Hannover, Hanover, Germany
[4] Norwegian Meteorological Institute, Oslo, Norway
[5] Institute of Geography and Geoecology, Karlsruhe Institute of Technology, Karlsruhe, Germany
[6] Pecanode GmbH, Germany
* Corresponding author: matthias.mauder@tu-dresden.de

With 8 figures and 1 table

Abstract: The imbalance between the measured available energy and the sum of the turbulent fluxes lead to the energy balance closure problem. In spite of several experimental and modelling studies, the reasons for the lack of closure are not fully understood, particularly, in a heterogeneous terrain. The LITFASS-2003 campaign in Northeastern Germany was designed to develop and to assess different area-averaging strategies of the surface fluxes over a heterogeneous land surface. The micrometeorological measurements of the campaign were targeted at local fluxes over different types of land surface that are essential to study the energy balance closure problem for a complex land surface where the secondary circulations induced by surface heterogeneity are suspected to influence the surface energy budget imbalance. To assess the influence of the secondary circulations we perform large-eddy simulations of a 5.4 × 5.4 km^2 sub-region of the LITFASS area with a flat topography and composed mainly of agricultural land. The boundary conditions for the simulation domain is derived from the experimental data collected on 30 May 2003. To capture the spatial variation of the fluxes, the surface fluxes of latent and sensible heat flux in the simulated domain are prescribed by composite fluxes derived from multiple surface flux stations operated during the experiment. A grid resolution of 1 m in the vertical and 2 m in the horizontal directions up to 72 m from the ground is achieved by employing a nested large-eddy simulation model. A total of five realizations of the domain is performed to calculate ensemble averages to separate the heterogeneity effect from the turbulence fluctuations and the 30-minute time-averaging ensures more representative statistics. We find the underestimation to be systematic and to increase with height. At a typical eddy covariance tower height of 10 m, we find the dispersive flux represents up to 5% of the prescribed surface fluxes, which partially explains the imbalance in the field measurements.

Keywords: Convective boundary layer; dispersive flux; energy balance closure; large-eddy simulation; secondary circulation

1 Introduction

Several experimental studies on the biosphere-atmosphere exchange show that the surface energy balance is not closed at most measurement sites (Wilson et al. 2002; Oncley et al. 2007; Franssen et al. 2010), i.e. the sum of the net radiation and the ground heat flux is not equal to the sum of the sensible and latent heat fluxes. Many reasons for this energy balance closure (EBC) problem are found in the literature, including instrumental errors, data processing errors and the lack of canopy heat storage terms. Mauder et al. (2020) review the many potential reasons for surface energy imbalance and discuss the challenges associated with measuring the turbulent fluxes. Growing evidence points to the inability of single tower measurements to capture the sub-mesoscale transport, where turbulent fluxes are systematically underestimated in the presence of secondary circulations. There is sufficient evidence to show that the horizontal flux divergence and the advection terms are not negligible in many cases (Moderow et al. 2007; De Roo & Mauder 2018; Wanner et al. 2022; Akinlabi et al. 2022; Zhou et al. 2023). A single tower measurement cannot capture the fluxes originating from a spatial

DOI: 10.1127/metz/2024/1213
Gebrüder Borntraeger Science Publishers, Stuttgart, www.borntraeger-cramer.com

covariation, so-called dispersive fluxes (Raupach & Shaw 1982), therefore a spatially-resolving multi-tower analysis needs to be performed to include the energy associated with dispersive fluxes induced by secondary circulations, which manifest locally as horizontal flux divergence and advection terms, e.g. Engelmann & Bernhofer (2016), Mauder et al. (2008) and Margairaz et al. (2020).

The flow in the atmospheric boundary layer (ABL) is generally turbulent. Therefore, high-frequency (> 10 Hz) measurements are necessary to capture this transport and analysis based on localized measurements rely on the validity of Taylor's frozen turbulence assumption to quantify vertical fluxes (Taylor 1938). However, in the presence of secondary circulations, which are a very common phenomenon during unstable stratification, this assumption is violated as these circulations are not propagated by the mean wind (Mahrt 1998). A convenient computational technique to study the spatial variability of turbulence in the ABL, is large-eddy simulation (LES). LES resolves the turbulence above a grid-dependent cutoff scale, below which the turbulence becomes more generic and can be (statistically) predicted by simpler models (Mason 1989). By this approach, the required computational resources are reduced in comparison to direct numerical simulations, while an accurate representation of the turbulence above the cutoff scale can be achieved. Kanda et al. (2004) were among the first to employ LES to study the EBC problem. Based on the virtual tower measurements in the dry simulation, they showed that a single tower measurements systematically underestimate the turbulent fluxes. They use the term "turbulent organized structure" and described the local advection effects associated with this kind of secondary circulations that are not captured by single tower measurements. Interestingly, they noted that weak thermal surface inhomogeneity in surface heating may lead to an improved closure, while stronger inhomogeneity leads to a poorer closure. The LES study of Steinfeld et al. (2007) further emphasized the need for spatially distributed measurements to overcome the limitations of single eddy-covariance tower measurements. They found the imbalance to be smaller than 5% for observation heights < 20 m, and then increasing with height. However, the imbalance is often significantly higher for near-surface field measurements and can exceed 30%. According to Inagaki et al. (2006), inhomogeneity in surface heating weakens turbulent organized structures (TOS) due to formation of thermally-induced mesoscale circulations (TMC) and at higher wind speeds, TOS are advected at sufficient speeds to maintain the validity of ergodicity assumption, which leads to a better EBC. Huang et al. (2008) found a set of non-dimensional functions to describe the dependence of flux imbalance on u_*/w_* and z/z_i, where u_*, w_* and z_i are friction velocity, convective velocity and boundary layer height respectively. They also investigated the effect of secondary circulations on the CO2 flux besides the fluxes of sensible and latent heat.

The EBC problem has also been investigated by dedicated experiments; the first one being the EBEX-2000 field campaign conducted in Central California (Oncley et al. 2007). This experiment was designed to quantify local advection amongst other possible explanations for a systematic bias in flux measurements. Hence, ten eddy-covariance towers were deployed over an area of approximated 1 km^2 over a cotton field, but this set-up was too small and homogeneous to measure significant advective fluxes. Another large-scale experiment with multiple eddy-covariance towers was the 'Lindenberg Inhomogeneous Terrain – Fluxes between Atmosphere and Surface: a long-term Study' campaign in 2003 (LITFASS-2003) in Brandenburg, Germany, around the boundary-layer test site Falkenberg of the German Meteorological Service (DWD). A special focus of this campaign was on the effect of surface heterogeneity on turbulent transport processes in an area of 10 km × 10 km (Beyrich & Mengelkamp 2006), and hence this experiment was also well-suited to study the EBC problem (Foken et al. 2010). More recently, Idealized Planar Array experiment for Quantifying Surface heterogeneity (IPAQS) campaign (Pardyjak et al. 2018) and the Chequamegon Heterogeneous Ecosystem Energy-Balance Study Enabled by a High-Density Extensive Array of Detectors 2019 (CHEESEHEAD19) campaign (Butterworth et al. 2021) deploy spatially distributed measurement towers to capture the effect of surface heterogeneities. Analysing the IPAQS dataset, Morrison et al. (2022) highlights the contribution of advection and dispersive fluxes that can be captured only with spatially distributed measurements or by realistic LES, which has been conducted by Wanner et al. (2024) for CHEESEHEAD19.

While previous studies on other sites (e.g. Eder et al. 2015) have already given indications for the reasons leading to a poor closure of the energy balance, using a combination of tower measurements and LES, these studies have been limited by the resolution of typically > 10 m to capture the turbulent behaviour closer to the surface. We address this limitation with the aid of a vertically nested grid (Huq et al. 2019) that allows us to achieve much higher grid spacing close to the surface, while still maintaining a sufficiently large domain to capture the low frequency turbulent organized structures over this LITFASS-2003 landscape. Maronga et al. (2014) noted that in their simulation, and in the previous studies for this area of Maronga & Raasch (2013) and Sühring & Raasch (2013), the fluxes from the single eddy-covariance stations were erroneously used to prescribe the lower boundary condition, which resulted in too strong surface fluxes. To overcome this issue, we use the composite fluxes derived from multiple energy balance stations over the same vegetation type as described in Beyrich et al. (2006). Hence, the aim of this study is to investigate the influence of secondary circulations on the flux measurement and the related lack of energy balance closure. To this end, we conduct a high-resolution LES study for a specific day

of the LITFASS-2003 campaign by using vertical grid nesting. These simulations will be driven by the composite fluxes derived from field measurements over all relevant land-cover types in the study area. We perform ensemble runs to separate heterogeneity effect from the turbulence fluctuations. In addition, we employ time-averaging to achieve more representative statistics of the virtual measurements.

In the following section, the LES tool and the simulation set-up are described along the data analysis steps. In Sect. 3 the results of the ensemble simulations are analysed both qualitatively and quantitatively. The influence of advection and flux divergence on the energy balance closure are then discussed in Sect. 4. Our findings are summarized along with recommendations for future analysis in Sect. 5.

2 Methods

2.1 The LES Model

The Parallelized Large-eddy simulation Model (PALM) version 4.0 (Subversion revision r2357) is used in this study (Raasch & Schröter 2001; Maronga et al. 2015). PALM discretises the non-hydrostatic incompressible Navier-Stokes equations in the Boussinesq approximation using the Finite Difference Method on a staggered Arakawa C grid (Arakawa & Lamb 1977). Prognostic equations for the components of the velocity field (u,v,w), potential temperature (θ) and humidity (q) are solved. In addition, PALM solves an equation for the sub-grid scale kinetic energy (e). The 1.5-order sub-grid-scale turbulence model based on Deardorff (1980) assumes the gradient-diffusion parameterisation modified by Moeng & Wyngaard (1988) and Saiki et al. (2000). The scalar and momentum advection terms are discretised by a fifth-order upwind scheme according to Wicker & Skamarock (2002). The lower boundary condition for the horizontal momentum equation is derived from Monin-Obukhov similarity theory (MOST). The six prognostic equations are integrated in time using a third-order Runge-Kutta scheme (Williamson 1980). The vertical grid-nesting method of Huq et al. (2019) is used to achieve higher resolution at reduced computational cost. This nested-LES method has previously been successfully employed by De Roo et al. (2018) to study the energy balance closure problem.

2.2 Set-up of high resolution vertically nested LES

The LITFASS-2003 experiment area encompasses several land-use classes, each having different roughness characteristics and varying surface heat flux. A complete description of the experiment site and the instrumentation set-up is available in Beyrich & Mengelkamp (2006). We selected a 5.4 × 5.4 km^2 area such that the measurement station A4 (maize), A5 (triticale), A6 (maize), and the tall tower station GM (grass) are well within the simulation domain since especially A6 was equipped with additional and higher quality instrumentation to measure the entire energy balance. We simulate a 3.5 hours period on the 30 May 2003 around noon; the local time is UTC+1. The chosen day was characterized by clear skies and weak Easterly geostrophic wind of 2 ms^{-1}. The former condition is ideal to avoid spatial variability in the incoming radiation and the weaker wind is still computationally feasible as higher wind speeds need smaller time steps. Considering the Easterly winds, the virtual towers are positioned at the Western side of the domain. The different land-use classes and the tower locations are shown in Fig. 1. The high resolution at the surface is made possible by vertical grid nesting, where a child grid at fine resolution sits within a parent grid at a coarser resolution. The coarse grid parent domain extends vertically up to 2212 m, the vertical resolution is kept constant at 3 m up to a height of 2000 m and thereafter the grid is stretched by a factor of 1.01. The vertical extent of the fine grid child domain is 72 m, the vertical grid resolution is kept constant at 1 m. The horizontal grid resolution of the coarse grid and the fine grid are 6 m and 2 m respectively. This corresponds to a grid nesting ratio of 3 in both horizontal and vertical directions. The total number of grid points in the parent and child grid are 583.2 × 10^6 and 486.72 × 10^6, respectively. Such large number of grid points demanded a total 2592 CPUs for one simulation. One simulation needed approximately 1 million core hours. The simulation parameters and grid configuration are listed in Table 1.

Periodic boundary conditions can be applied in the lateral dimensions as the horizontal extent of the parent and the child grid are identical. This allows the Poisson equation for pressure to be solved with a computationally efficient Fast Fourier Transform algorithm. The velocity at the bottom is set to Dirichlet condition corresponding to zero vertical and horizontal velocity. The vertical velocity at the top of the parent domain is zero and the horizontal velocity is equal to the geostrophic wind. For the scalar quantities, namely potential temperature, humidity, turbulent kinetic energy, and pressure, we apply Neumann conditions at the bottom and at the top. The top boundary conditions for the child grid are interpolated from the parent grid (Huq et al. 2019). In the employed two-way nesting approach the coarse grid is updated by “anterpolation” (feedback) from the fine grid after each time step.

The surface roughness for each land-use class is obtained from the Coordinated Information on the European Environment (CORINE) dataset, published by the European Environment Agency, modified by Maronga & Raasch (2013). However, the roughness length of the forest had to be reduced from the original 1.5 m to 0.45 m to comply with the requirements of MOST where the roughness length cannot be more than half the vertical grid spacing. The surface values of potential temperature, humidity, sensible heat flux and latent heat flux too vary depending on the land-use type. The

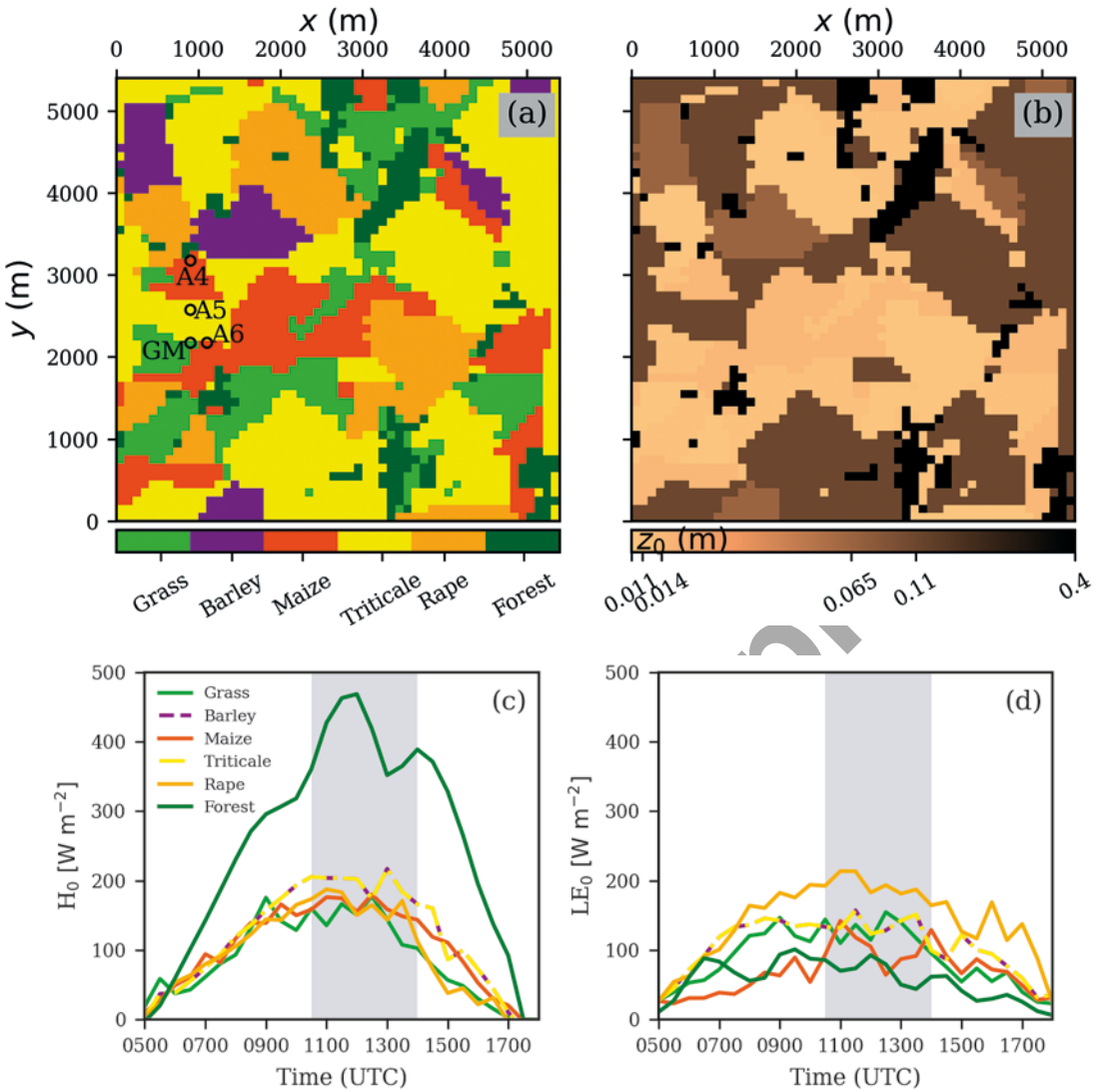

Fig. 1. The vegetation classification derived from the CORINE dataset for the simulated area with the position of the virtual towers corresponding to the in-situ measurement towers indicated by labels A6, A4, GM and A5 (a) and roughness length (b). The interpolated time series of composite fluxes of sensible (c) and latent (d) heat fluxes at the surface on 30 May 2003; the shaded portion indicates the period simulated in this study. Barley and Triticale are grouped together in composite flux calculation, however, the roughness lengths of the two vegetation are not identical.

surface fluxes available at 30-minute intervals were linearly interpolated in time during the duration of the simulation as shown in Fig. 1. A variable time step was allowed up to a spin-up phase of 3 hours where PALM computes a time step such that the Courant-Friedrichs-Lewy (CFL) condition is satisfied in both the grids. In the last 30 minutes of the simulation a conservative fixed time step of 0.05 s is prescribed. To initiate the onset of convection it is common practice in LES codes to impose perturbations on initial arrays. In PALM it is common to impose perturbations onto the horizontal velocity fields. In the PALM version utilized for this study, uniformly distributed random numbers are generated using a predefined integer seed for Fortran's built-in random number generator, while the seed changed for each of the ensemble runs, following Maronga & Raasch (2013). This guarantees that ensemble runs are statistically independent. The maximum amplitude of the perturbation is set to 0.25 ms^{-1}. The perturbation energy, defined as the resolved-scale turbulent kinetic energy, is restricted to 0.01 m^2 s^{-2}, in order to make sure that the random perturbations only trigger initial turbulence development and have no impact during daytime convective conditions. Additionally, numerical round-off errors

Table 1. Grid configuration and simulation parameters.

Simulation Parameters	Value
Parent domain size	5.4 × 5.4 × 2.2 km^3
Child domain size	5.4 × 5.4 × 0.072 km^3
Parent grid resolution (dx,dy,dz)	6 m, 6 m, 3 m
Child grid resolution (dx,dy,dz)	2 m, 2 m, 1 m
Surface heat flux, H_0	time-varying interpolated composite fluxes following Beyrich et al. (2006) (Fig. 1(c))
Surface humidity flux, LE_0	time-varying interpolated composite fluxes following Beyrich et al. (2006) (Fig. 1(d))
Geostrophic wind	$u_g = -2$ m s^{-1} (Easterly), $v_g = 0$ m s^{-1}
Roughness length	depending on vegetation type from CORINE dataset (Fig. 1(b))
Density, ρ	1.204 Kg K^{-1}
Specific heat of air, C_p	1005 J Kg^{-1} K^{-1}
Latent heat of vaporization, L_v	2.5 · 10^6 J Kg^{-1}
Simulated time	12600 s (10:30 UTC - 14:00 UTC)
Spin-up time	10800 s (13:30 UTC - 13:30 UTC)
Data capture and temporal-averaging interval	1800 s (13:30 UTC - 14:00 UTC)
Number of realizations for ensemble statistics	5

arising from compiler optimization can also adversely affect the reproducibility of ensemble members. To enable faster computation, the default compiler settings may allow floating point operations to be imprecise. Appropriate compiler specific options are needed when compiling the model to ensure that the double-precision floating-point operations are numerically exact and the simulations remain deterministic for the prescribed random seed. Langkamp & Böhner (2011) analyse the influence of compiler on Weather Research and Forecast model and note that non value-safe optimizations can result in different model outputs. The five realizations of the domain are referred to as LIT-A, LIT-B, LIT-C, LIT-D and LIT-E in the following sections.

2.3 Data Post-Processing and analysis

The energy balance ratio (EBR) represents the amount of simulated turbulent flux to the prescribed surface flux. In equation 2.1, w, θ and q are vertical velocity, potential temperature and humidity, respectively. The first term in the numerator is the measured sensible heat flux and the second term is the latent heat flux. In the denominator, H_0 and L_0 represent the surface sensible and latent heat fluxes, respectively,

$$\mathrm{EBR} = \frac{\rho \cdot C_p \cdot \overline{w'\theta'} + \rho \cdot L_v \cdot \overline{w'q'}}{H_0 + LE_0}; \qquad (2.1)$$

where ρ, C_p and L_v are air density, specific heat of air and latent heat of vaporization, respectively. EBR is calculated for each grid point using time-averaged H_0 and L_0 of the corresponding horizontal grid point at the surface. Since time-averaged turbulent flux was not a standard output in PALM 4.0, a user extension to the standard code was employed to calculate the total flux at each time step and only the time-averaged total flux is written at the end of each simulation. The term w"θ" represents the sub-grid scale flux and the overbar denotes time-averaging.

$$\overline{w\theta} = \overline{w \cdot \theta + w"\theta"}. \qquad (2.2)$$

The sensible heat flux can then be calculated from the total flux, $\overline{w}$ and $\overline{\theta}$ as

$$\overline{w'\theta'} = \overline{w\theta} - \overline{w} \cdot \overline{\theta}. \qquad (2.3)$$

The dispersive sensible flux (H_{disp}) can then be computed as,

$$\langle \overline{w} * \overline{\theta} * \rangle = \langle (\overline{w} - \langle \overline{w} \rangle) \cdot (\overline{\theta} - \langle \overline{\theta} \rangle) \rangle; \qquad (2.4)$$

where the angle brackets indicate horizontal spatial mean and the asterisk indicates deviation from the spatial mean. Similarly, the vertical latent heat fluxes and dispersive latent heat fluxes (LE_{disp}) are calculated by replacing θ with specific humidity, q in Eqs. 2.3 and 2.4. The ensemble fluxes are computed as arithmetic mean of the member runs (Eqs. 2.5 and 2.6) and the kinematic vertical fluxes are convert to dynamic fluxes,

$$H_{ens} = \rho \cdot C_p \cdot \frac{1}{N} \sum_{i=1}^{N} \overline{w'\theta'}_i, \qquad (2.5)$$

$$LE_{ens} = \rho \cdot L_v \cdot \frac{1}{N} \sum_{i=1}^{N} \overline{w'q'}_i. \qquad (2.6)$$

Since the 30-min averaged surface flux in the denominator of equation 2.1 is identical in all the runs, the ensemble EBR (Eq. 2.7) is also computed as arithmetic mean,

$$EBR_{ens} = \frac{1}{N}\sum_{i=1}^{N} EBR_i. \qquad (2.7)$$

3 Results

We present a brief qualitative analysis before presenting the statistical analysis of the simulations in order to demonstrate the plausibility of the simulations. All the results presented in this section are time-averaged over the last 30 minutes of the simulated period. All results are obtained from the nested child grid. The vertical velocity contours of an XZ-plane cutting across the A6 site are shown in Fig. 2. There are noticeable differences in the up and down drafts patterns between the multiple realizations even after time-averaging. The structures are even noticeable in the ensemble contour. This supports the prevalent hypothesis of the secondary circulation as the cause of the energy balance closure problem; the single-tower EC systems cannot capture these persistent circulations.

The three-dimensional velocity vector plotted at a height of 10 m and coloured by the velocity magnitude in Fig. 3 shows that the vectors are predominantly oriented in the direction of the mean wind, but with noticeable areas of convergence and divergence. Particularly, in the northern section of the domain, we observe a convergence zone characterized by low velocity magnitude that is typical of a roll-like structure. A similar convergence zone is also noticeable in the region close to the A6 towers. These roll-like structures are related to physical mechanisms in the convective boundary layer, rather than artificial structures associated with the Tollmien–Schlichting waves that emerge as the flow transitions from laminar to turbulent and could be persistent under periodic boundary conditions and near-neutral conditions. We allow a sufficient spin-up time for turbulence to develop and, more importantly, the large thermals in convective conditions ensure such artificial structures do not persist in the simulation domain. The formation of roll-like structures at higher mean wind speeds, with axis aligned to the mean flow, have also been observed by Maronga & Raasch (2013) in their LITFASS-2003 simulations and by Margairaz et al. (2020) in their simulations with idealized heterogeneities. Nevertheless, roll-like and cellular circulation structures are possible even above homogeneous surface due to self-organization of turbulence (Etling & Brown 1993; De Roo & Mauder 2018).

The time- and ensemble-averaged horizontal distribution of w, θ and q are shown in Fig. 4 for multiple vertical levels in the surface layer. Region of higher w indicating strong updraft is noticeable in the northern section, at all vertical

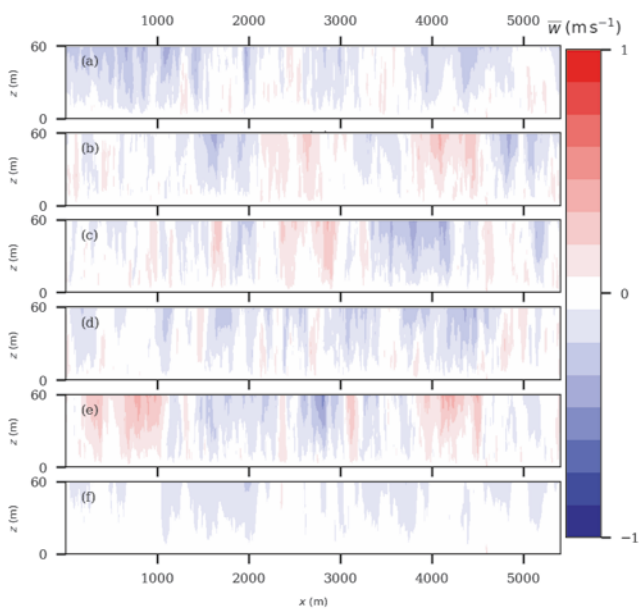

Fig. 2. The time-averaged vertical velocity of the XZ plane cross-section cutting across the A6 measurement site. Panels from top to bottom correspond to realizations LIT-A, LIT-B, LIT-C, LIT-D, LIT-E and the ensemble averaged $\overline{w}$ of the five realizations, respectively. Persistent secondary circulation are present even after temporal and ensemble averaging.

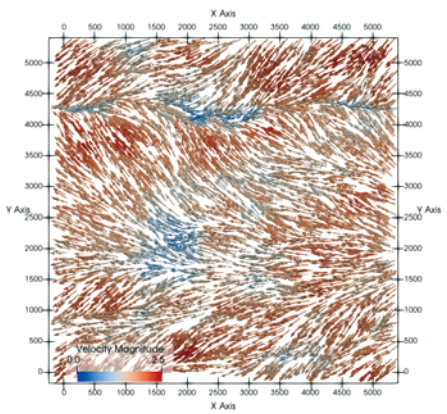

Fig. 3. The time-averaged three-dimensional velocity vectors of a horizontal slice at 10 m height coloured by the velocity magnitude. The convergence zone characterized by low velocity magnitude in the northern section, is typical of a roll like structure's updraft. Similarly, the divergence zone in the southern section is characteristic of a downdraft. Child grid output of one realization (LIT-C) is shown.

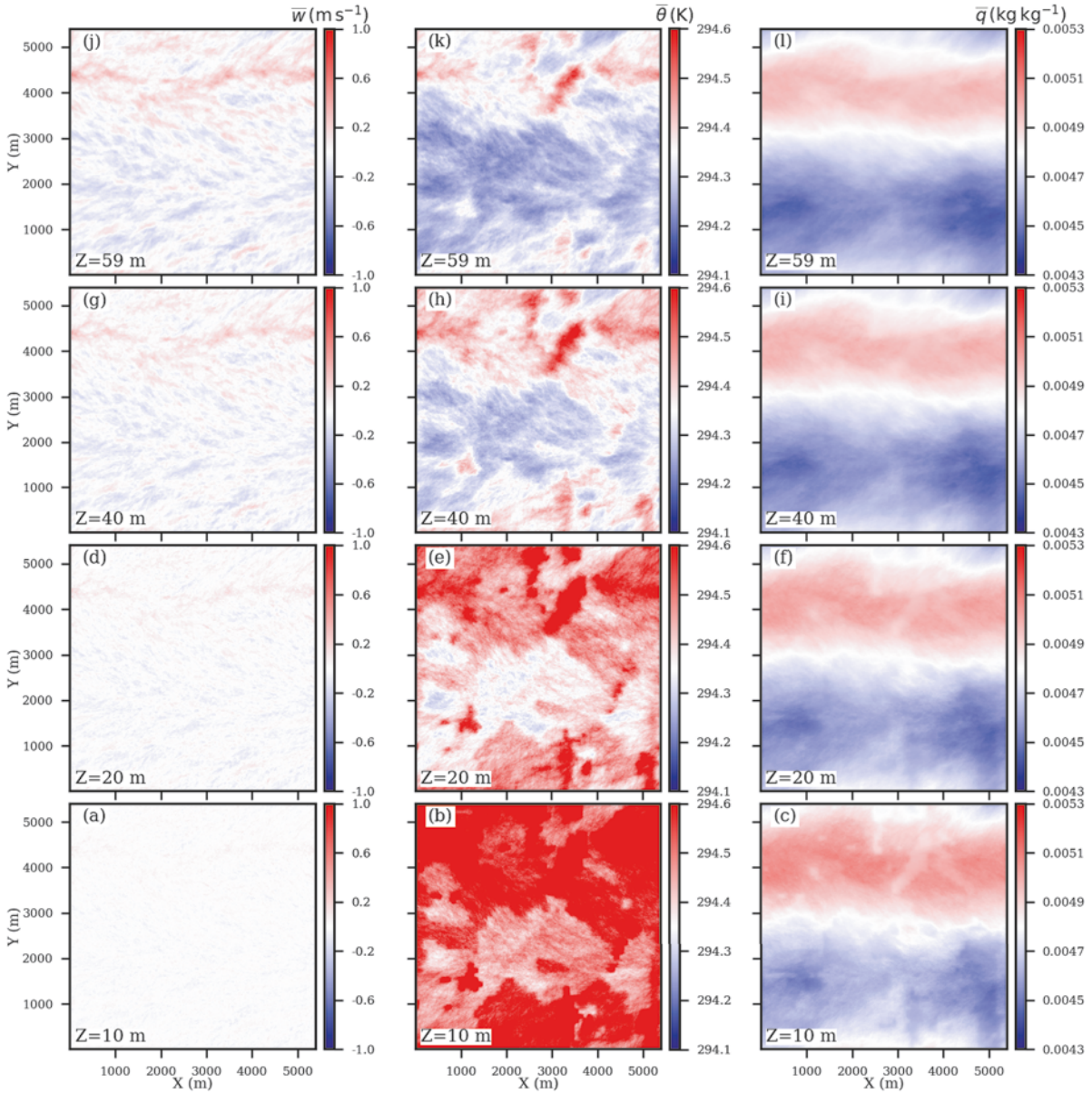

Fig. 4. The time-averaged and ensemble-averaged vertical velocity, potential temperature and specific humidity, from left to right, at multiple XY slices are shown. Panels from bottom to top correspond to vertical levels 10 m, 20 m, 40 m, and 59 m, respectively. The updraft in the northern section is noticeable from vertical velocity for all vertical levels.

levels. This corresponds to the location of convergence zone observed in Fig. 3. The θ at lower levels have strong signature of the underlying surface. At higher levels, θ starts to be more evenly distributed, but the forest sites continue to be warmer than the surrounding region. Specific humidities q at all levels are higher in the northern section and lower in the southern. The updraft zone is relatively narrow and humid whereas the downdraft zone is broad and dry. As seen in Fig. 1, there are more patches in the northern section with higher surface roughness and larger surface sensible heat flux, which are likely factors resulting in the convective updrafts carrying humidity away from the surface. On the other hand, the downdrafts transport dry air towards the surface from aloft.

The sensible and latent heat flux, and energy balance ratio at a height of 10 m are shown in Fig. 5 for an arbitrary realization LIT-C and for the ensemble of all realizations. The spatial plots of sensible and latent heat fluxes at a height of 10 m, in Fig. 5(a) and Fig. 5(b), shows that the fluxes correlate with the surface heterogeneity even at this height. This is in accordance with Maronga & Raasch (2013) were they investigated the influence of the blending height

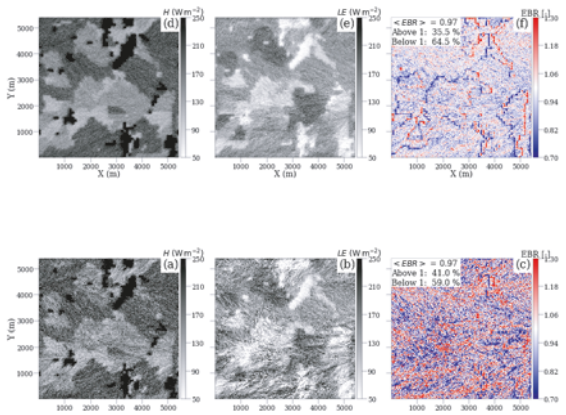

Fig. 5. Time-averaged sensible heat flux, latent heat flux and EBR at a height of 10 m; for one realization LIT-C (top) and for the ensemble average of realizations (bottom). Areas of under- and overestimation near the edge of land-use classes are pronounced in ensemble EBR (f).

for the same day as in this study. The pattern of the fluxes still appears noisy; this is because the turbulent fluctuations that superimpose the mean fluxes have not vanished even after 30-min time-averaging. In comparison, the fluxes of Fig. 5(d) and Fig. 5(e) are less noisy as the ensemble averaging has removed some of the fluctuations that still remained after time-averaging. The effect of the ensemble average is evident in Fig. 5(f) where the EBR clearly shows the edge-effects in the areas where there is change in surface heterogeneity. On the contrary, the edge effects in realization LIT-C in Fig. 5(c) are less obvious. Areas of overclosure, underclosure, and regions of ideal closure are distributed throughout the horizontal slice. But at some regions, like the forest patch in the northern section, the edge effects are distinct even in LIT-C. As annotated in Fig. 5(f) the horizontally averaged EBR of the ensemble domain at 10 m is 0.97. Interestingly, the horizontally averaged EBR of LIT-C and the ensemble remains the same even as the observed pattern is considerably different. Since the region upstream of the forest patch has a surface type with smaller fluxes, underclosure at the upstream edge is expected as the reference flux for the EBR calculation is the higher prescribed flux of the forest. Likewise, overclosure is expected at the downstream edge. The overclosure and underclosure due to edge effects should typically cancel out when averaged over the entire domain. However, due to secondary circulations the imbalance persists in the horizontal averaged EBR.

The spatial variability of the fluxes and the energy balance ratio are visualized with the help of histogram of the ensemble in Fig. 6. The histogram for different levels show that the vertical fluxes decreases with height and the median lies below one in all cases. The EBR histograms have similar shape as those for the sensible heat flux. The tails of histograms to the left indicate that the underclosure is systematic with strong dependence on the height. Whereas the tails on the right show that the overclosure is not systematic and not dependent on the height. However, the tails of the latent heat flux histograms show dependence with height both above and below one.

Dispersive fluxes, which represent the vertical transport by secondary circulations, normalized by the surface flux (Fig. 7) indicate that both H_{disp} and LE_{disp} increase with height for all ensemble members. However, the increase of LE_{disp} is stronger than that of H_{disp} and stays stronger over longer vertical distance. However, such increase with height is not observed in the humidity profile (data not shown). The slope of the time-averaged humidity profile was found to be similar to the potential temperature profile.

The ensemble-averaged vertical profiles of sensible and latent heat flux at A6, A4, GM and A5 sites are shown in Fig. 8 (a,b,c and d) and the vertical profiles of EBR are shown in Fig. 8 (e,f,g and h), respectively. The results of the bottom 5 m of the simulation are not shown as the turbulent transport in the lowest levels exhibit significant contributions from the parameterised subgrid-scale fluxes rather than the resolved scales. At all sites sensible heat flux is greater than the latent heat flux. The turbulent flux profile at the A6 feature considerable differences compared to GM even though both sites are only a few meters apart. These differences are also noticeable in the EBR, while A6 has a slight overclosure, underclosure dominates above 20 m at the GM site.

4 Discussion

It is pertinent to discuss the general limitations of the large-eddy simulations before interpreting the results. The primary limitations arises at the lower boundary where MOST is widely used in all atmospheric models, including majority of the LES models. A detailed discussion on the applicability and limitation of MOST can be found in Foken (2006), Basu & Lacser (2017), Maronga et al. (2020) and Stiperski & Calaf (2023). The roughness length of the forest had to be reduced in this study since the vertical grid spacing is smaller than the roughness length. Wanner et al. (2022) studied the influence of choice of lower boundary conditions on the development of dispersive fluxes and show that reduced roughness length could lead to lower dispersive flux compared to a simulation employing plant canopy model. Nevertheless, they find the results of simulations using prescribed surface fluxes and reduced roughness length were still reasonable. Since the turbulence in the near-wall region is parameterised, we avoid discussing the results in lowest grid levels. We focus our discussion at 10 m – a typical measurement height of the eddy covariance towers. The second limitation in LES studies is the grid resolution. While it is crucial to achieve high vertical resolution, the aspect ratio should not be compromised. Previous LES studies on Energy Balance Closure

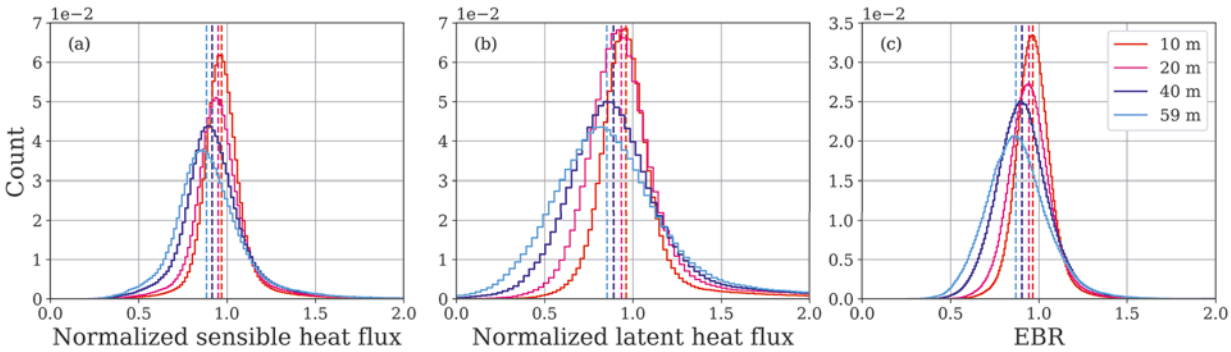

Fig. 6. Histogram at different height levels describing the horizontal variability of the ensemble-averaged sensible heat flux (a) and latent heat flux (b). Heat fluxes at every grid point is normalized by the time-averaged surface flux of the respective grid point at the surface. The histogram of the ensemble-averaged EBR is shown in (c). The median (dashed lines) is below one in all cases. The left tail and peak of histogram (c) shows underestimation is systematic with dependence on height.

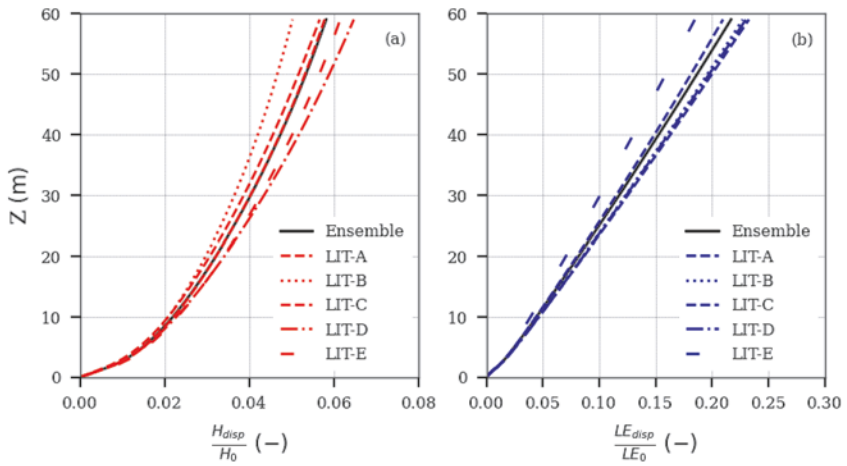

Fig. 7. Dispersive sensible (a) and latent (b) heat fluxes normalized by surface fluxes. Both H_{disp} and LE_{disp} increase with height for all realizations but LE_{disp} shows stronger increase with height.

have been restricted by the vertical grid resolution, preventing the visualization of the structures near the surface layer (De Roo et al. 2018). Our simulation with 1 m and 2 m resolution in the vertical and horizontal directions respectively makes it computationally feasible without compromising on low aspect ratio that is ideally needed by the isotropic subgrid model. The vector field in Fig. 3(a) qualitatively shows the turbulence structures resolved at 10 m made possible by increased resolution. The peak boundary layer height (Z_i) observed in our simulation is 1250 m. This is lower than the 1800 m Z_i observed by Maronga & Raasch (2013) for same time of the day. The lower Z_i in our simulation could be partially due to the use of composite fluxes which are not as strong as the tower fluxes used by Maronga & Raasch (2013).

Another limitation often overlooked is the need for multiple realizations of the simulation domain. The spread of the ensemble member noticeable in Fig. 7 is a clear indication that one realization of the domain is not sufficient. Ensemble statistics calculated from multiple realizations provide better confidence. While higher number of realizations provide better statistics, we have to acknowledge the computational resource limitations in achieving ideal statistics.

In Fig. 7, the simulated dispersive fluxes at 10 m height account for 2% and 5% of the sensible and latent heat flux at the surface, respectively. The roll-like secondary circulations arising from the humid updraft and the dry downdraft, observed in Fig. 3 and Fig. 4, generate these dispersive fluxes. Comparing the horizontal distribution of θ and q, we can see that the humidity distribution is aligned with the up- and

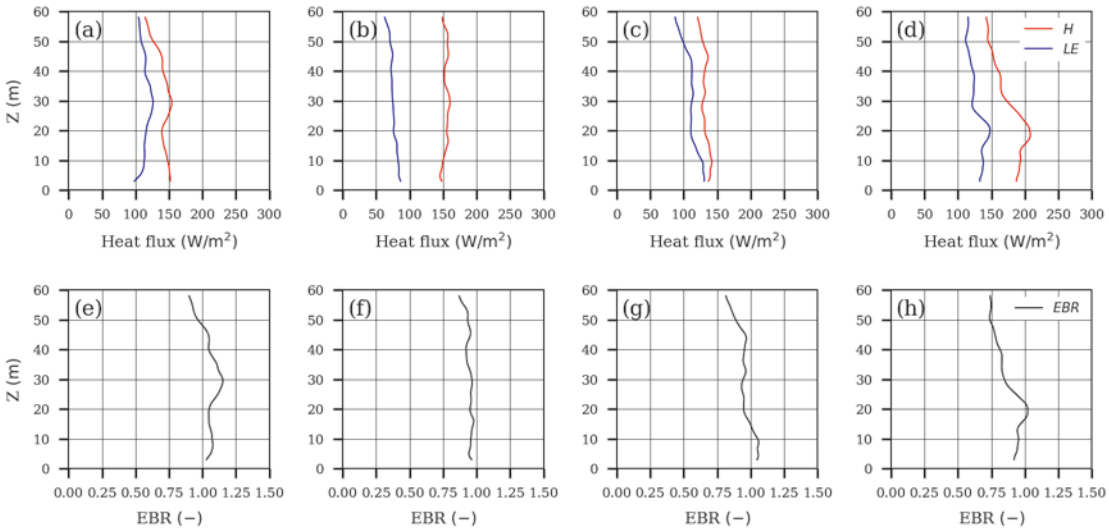

Fig. 8. Time-averaged and ensemble-averaged vertical profile of turbulent heat fluxes (top) and EBR (bottom); from left to right for sites A6 (Maize), A4 (Maize), GM (Grass) and A5 (Triticale). In all cases, *H* is greater than *LE*. There are noticeable differences between A6 and GM even though the virtual towers are only a few meters apart.

downdrafts while θ exhibits the surface characteristics. The coherent bands of q as compared to θ can be considered as the reason for higher LE_{disp}. None of the previously conducted LES studies on the EBC problem found any significant underestimation at 10 m height due to their limited grid resolution. Nevertheless, the range of dispersive flux in this study is still much smaller than the imbalance of the actual field measurements. This discrepancy could either mean that the grid resolution of our simulation is still not sufficient, or that the imbalance from the field measurements has also other reasons than transport by secondary circulations, e.g. neglected storage terms (heat or biochemical), instrumental biases, mismatch of flux footprints etc., which can potentially affect the magnitude of the energy balance residual. Additionally, LES using prescribed fluxes, as in this study, cannot capture the feedback between secondary circulation and the surface temperature via convergence and divergence zones. A coupled land-surface model should be employed to include such second-order effects (Wanner et al. 2022). In most of our virtual tower measurements, the imbalance increases with height, which is in accordance with previous studies (Kanda et al. 2004; Huang et al. 2008) and with our understanding of the underlying process of secondary circulations that weaken in intensity towards the ground.

Regarding the partitioning of the residual, De Roo et al. (2018) found larger underestimation of sensible heat flux than the latent heat flux in the surface layer in an idealized simulation of homogeneous terrain. While we are unable to fully explain the reason for higher dispersive flux of latent heat, we suspect that entrainment of dry air could be a factor causing a different response to secondary circulations in comparison to the transport of sensible heat. The LES studies of Maronga & Raasch (2013) and Uhlenbrock et al. (2004) also found a greater contribution of the mesoscale fluxes to the latent heat flux for the same LITFASS-2003 experiment. Charuchittipan et al. (2014) studied the effect of the averaging time of eddy covariance measurements on the energy balance closure for the LITFASS-2003 campaign. Using wavelet analysis, they found that warm updrafts in secondary circulations mostly transport sensible heat and longer-averaging time captures more of the missing energy. Since only a 30-minute period is analysed in this study, the low-frequency variation of the heat flux could not be evaluated. For a heterogeneous landscape in Canada, Eder et al. (2014) report equal partitioning of the mesoscale energy transport between the sensible and the latent hear flux. Therefore, it seems that the partitioning of the residual depends on the specific distribution of land-cover types, low frequency contributions, and perhaps also on the meteorological conditions.

5 Conclusions

We presented a high-resolution LES designed and analysed to study energy balance closure in a heterogeneous farmland-dominated landscape. We chose the LITFASS-2003 experiment to conduct these simulations because of the wealth of observations and LES studies previously conducted for the same study area. This allows us to compare our results with a consolidated set of different kinds of data. We isolated heterogeneity effects from the turbulence fluctuations by calculating ensemble averages. Consistent with some previous studies, we found evidence to support secondary circulations to be a significant cause of the lack of closure observed in

field campaigns, as the associated vertical transport cannot be measured by EC towers. In contrast to previously published studies, we have investigated the effect of these circulations on virtual EC measurements with an unprecedented vertical resolution of 1 m in the vertical and 2 m in the horizontal direction, which allows for more a realistic representation of characteristic features of the turbulent flow near the surface.

The calculated ensemble of the dispersive fluxes show that this otherwise often neglected vertical transport increases with height and at a height of 10 m, they account for up to 5% of the prescribed surface fluxes of sensible and latent heat. While this is an evidence of energy that cannot be measured by approaches assuming Taylor's frozen hypothesis, such as single-tower EC, the magnitude of this systematic bias is still low compared to the total imbalance at many sites, which is on the order of 15% on average (Foken et al. 2010; Stoy et al. 2013). We also found evidence to support the notion that the underclosure occurs more frequently than overclosure with a strong dependence on the height. The underclosure increases to a value of up to 15% for a height of 60 m.

Future studies designed to study the energy balance closure problem should aim to achieve even higher resolution to fully understand the full contribution of the dispersive fluxes to the imbalance. A land-surface model should be employed at the lower boundary condition to allow for potential feedbacks between secondary circulations and surface fluxes. It is also essential to consider the other terms, such as storage and local advection, that are not included in our analysis. A control volume approach, as used by De Roo & Mauder (2018) and Eder et al. (2015), may provide more insight on the energy partitioning. Lastly, flux footprint analyses may lead to a better comparison of the virtual measurements with the turbulence measured in the field.

Acknowledgements: This work was conducted within the Helmholtz Young Investigators Group "Capturing all relevant scales of biosphere-atmosphere exchange – the enigmatic energy balance closure problem", which is funded by the Helmholtz-Association through the President's Initiative and Networking Fund, and by KIT. Computer resources for this project have been provided by the Leibniz Supercomputing Centre under grant: pr48la. We also gratefully acknowledge Frank Beyrich (German Meteorological Service) for suggestions on a previous version of this manuscript.

References

Akinlabi, E., Maronga, B., Giometto, M. G., & Li, D. (2022). Dispersive fluxes within and over a real urban canopy: A large-eddy simulation study. *Boundary-Layer Meteorology, 185*(1), 93–128. https://doi.org/10.1007/s10546-022-00725-6

Arakawa, A., & Lamb, V. R. (1977). Computational design of the basic dynamical processes of the UCLA general circulation model. In *Methods in Computational Physics: Advances in Research and Applications* (pp. 173–265). Elsevier; https://doi.org/10.1016/B978-0-12-460817-7.50009-4

Basu, S., & Lacser, A. (2017). A cautionary note on the use of monin–obukhov similarity theory in very high-resolution large-eddy simulations. *Boundary-Layer Meteorology, 163*(2), 351–355. https://doi.org/10.1007/s10546-016-0225-y

Beyrich, F., & Mengelkamp, H. T. (2006). Evaporation over a heterogeneous land surface: EVA_GRIPS and the LITFASS-2003 experiment – an overview. *Boundary-Layer Meteorology, 121*(1), 5–32. https://doi.org/10.1007/s10546-006-9079-z

Beyrich, F., Leps, J. P., Mauder, M., Bange, J., Foken, T., Huneke, S., … Zittel, P. (2006). Area-averaged surface fluxes over the litfass region based on eddy-covariance measurements. *Boundary-Layer Meteorology, 121*(1), 33–65. https://doi.org/10.1007/s10546-006-9052-x

Butterworth, B. J., Desai, A. R., Townsend, P. A., Petty, G. W., Andresen, C. G., Bertram, T. H., … Wilczak, J. M. (2021). Connecting land–atmosphere interactions to surface heterogeneity in cheesehead. *Bulletin of the American Meteorological Society, 102*(2), E421–E445. https://doi.org/10.1175/BAMS-D-19-0346.1

Charuchittipan, D., Babel, W., Mauder, M., Leps, J. P., & Foken, T. (2014). Extension of the averaging time in eddy-covariance measurements and its effect on the energy balance closure. *Boundary-Layer Meteorology, 152*(3), 303–327. https://doi.org/10.1007/s10546-014-9922-6

De Roo, F., & Mauder, M. (2018). The influence of idealized surface heterogeneity on virtual turbulent flux measurements. *Atmospheric Chemistry and Physics, 18*(7), 5059–5074. https://doi.org/10.5194/acp-18-5059-2018

De Roo, F., Zhang, S., Huq, S., & Mauder, M. (2018). A semi-empirical model of the energy balance closure in the surface layer. *PLoS One, 13*(12), e0209022. https://doi.org/10.1371/journal.pone.0209022

Deardorff, J. W. (1980). Stratocumulus-capped mixed layers derived from a three-dimensional model. *Boundary-Layer Meteorology, 18*(4), 495–527. https://doi.org/10.1007/BF00119502

Eder, F., Schmidt, M., Damian, T., Träumner, K., & Mauder, M. (2015). Mesoscale eddies affect near-surface turbulent exchange: Evidence from lidar and tower measurements. *Journal of Applied Meteorology and Climatology, 54*(1), 189–206. https://doi.org/10.1175/JAMC-D-14-0140.1

Eder, F., de Roo, F., Kohnert, K., Desjardins, R. L., Schmid, H. P., & Mauder, M. (2014). Evaluation of two energy balance closure parametrizations. *Boundary-Layer Meteorology, 151*(2), 195–219. https://doi.org/10.1007/s10546-013-9904-0

Engelmann, C., & Bernhofer, C. (2016). Exploring eddy-covariance measurements using a spatial approach: The eddy matrix. *Boundary-Layer Meteorology, 161*(1), 1–17. https://doi.org/10.1007/s10546-016-0161-x

Etling, D., & Brown, R. A. (1993). Roll vortices in the planetary boundary layer: A review. *Boundary-Layer Meteorology, 65*(3), 215–248. https://doi.org/10.1007/BF00705527

Franssen, H. H., Stöckli, R., Lehner, I., Rotenberg, E., & Seneviratne, S. (2010). Energy balance closure of eddy-covariance data: A multisite analysis for european FLUXNET stations. *Agricultural and Forest Meteorology, 150*(12), 1553–1567. https://doi.org/10.1016/j.agrformet.2010.08.005

Foken, T. (2006). 50 years of the monin–obukhov similarity theory. *Boundary-Layer Meteorology, 119*(3), 431–447. https://doi.org/10.1007/s10546-006-9048-6

Foken, T., Mauder, M., Liebethal, C., Wimmer, F., Beyrich, F., Leps, J. P., … Bange, J. (2010). Energy balance closure for the LITFASS-2003 experiment. *Theoretical and Applied Climatology, 101*(1-2), 149–160. https://doi.org/10.1007/s00704-009-0216-8

Huang, J., Lee, X., & Patton, E. G. (2008). A modelling study of flux imbalance and the influence of entrainment in the convective boundary layer. *Boundary-Layer Meteorology, 127*(2), 273–292. https://doi.org/10.1007/s10546-007-9254-x

Huq, S., De Roo, F., Raasch, S., & Mauder, M. (2019). Vertically nested LES for high-resolution simulation of the surface layer in PALM (version 5.0). *Geoscientific Model Development, 12*(6), 2523–2538. https://doi.org/10.5194/gmd-12-2523-2019

Inagaki, A., Letzel, M. O., Raasch, S., & Kanda, M. (2006). Impact of surface heterogeneity on energy imbalance: A study using LES. *Journal of the Meteorological Society of Japan, 84*(1), 187–198. https://doi.org/10.2151/jmsj.84.187

Kanda, M., Inagaki, A., Letzel, M. O., Raasch, S., & Watanabe, T. (2004). LES study of the energy imbalance problem with eddy covariance fluxes. *Boundary-Layer Meteorology, 110*(3), 381–404. https://doi.org/10.1023/B:BOUN.0000007225.45548.7a

Langkamp, T., & Böhner, J. (2011). Influence of the compiler on multi-cpu performance of wrfv3. *Geoscientific Model Development, 4*(3), 611–623. https://doi.org/10.5194/gmd-4-611-2011

Mahrt, L. (1998). Flux sampling errors for aircraft and towers. *Journal of Atmospheric and Oceanic Technology, 15*(2), 416–429. https://doi.org/10.1175/1520-0426(1998)015<0416:FSEFAA>2.0.CO;2

Margairaz, F., Pardyjak, E. R., & Calaf, M. (2020). Surface thermal heterogeneities and the atmospheric boundary layer: The relevance of dispersive fluxes. *Boundary-Layer Meteorology, 175*(3), 369–395. https://doi.org/10.1007/s10546-020-00509-w

Maronga, B., & Raasch, S. (2013). Large-eddy simulations of surface heterogeneity effects on the convective boundary layer during the LITFASS-2003 experiment. *Boundary-Layer Meteorology, 146*(1), 17–44. https://doi.org/10.1007/s10546-012-9748-z

Maronga, B., Hartogensis, O. K., Raasch, S., & Beyrich, F. (2014). The effect of surface heterogeneity on the structure parameters of temperature and specific humidity: A large-eddy simulation case study for the LITFASS-2003 experiment. *Boundary-Layer Meteorology, 153*(3), 441–470. https://doi.org/10.1007/s10546-014-9955-x

Maronga, B., Gryschka, M., Heinze, R., Hoffmann, F., Kanani-Sühring, F., Keck, M., … Raasch, S. (2015). The parallelized large-eddy simulation model (palm) version 4.0 for atmospheric and oceanic flows: Model formulation, recent developments, and future perspectives. *Geoscientific Model Development, 8*(8), 2515–2551. https://doi.org/10.5194/gmd-8-2515-2015

Maronga, B., Knigge, C., & Raasch, S. (2020). An improved surface boundary condition for large-eddy simulations based on monin–obukhov similarity theory: Evaluation and consequences for grid convergence in neutral and stable conditions. *Boundary-Layer Meteorology, 174*(2), 297–325. https://doi.org/10.1007/s10546-019-00485-w

Mason, P. J. (1989). Large-eddy simulation of the convective atmospheric boundary layer. *Journal of the Atmospheric Sciences, 46*(11), 1492–1516. https://doi.org/10.1175/1520-0469(1989)046<1492:LESOTC>2.0.CO;2

Mauder, M., Desjardins, R. L., Pattey, E., Gao, Z., & Van Haarlem, R. (2008). Measurement of the sensible eddy heat flux based on spatial averaging of continuous ground-based observations. *Boundary-Layer Meteorology, 128*(1), 151–172. https://doi.org/10.1007/s10546-008-9279-9

Mauder, M., Foken, T., & Cuxart, J. (2020). Surface-energy-balance closure over land: A review. *Boundary-Layer Meteorology, 177*(2-3),395–426.https://doi.org/10.1007/s10546-020-00529-6

Moeng, C. H., & Wyngaard, J. C. (1988). Spectral analysis of large-eddy simulations of the convective boundary layer. *Journal of the Atmospheric Sciences, 45*(23), 3573–3587. https://doi.org/10.1175/1520-0469(1988)045<3573:SAOLES>2.0.CO;2

Moderow, U., Feigenwinter, C., & Bernhofer, C. (2007). Estimating the components of the sensible heat budget of a tall forest canopy in complex terrain. *Boundary-Layer Meteorology, 123*(1), 99–120. https://doi.org/10.1007/s10546-006-9136-7

Morrison, T., Pardyjak, E. R., Mauder, M., & Calaf, M. (2022). The heat-flux imbalance: The role of advection and dispersive fluxes on heat transport over thermally heterogeneous terrain. *Boundary-Layer Meteorology, 183*(2), 227–247. https://doi.org/10.1007/s10546-021-00687-1

Oncley, S. P., Foken, T., Vogt, R., Kohsiek, W., DeBruin, H. A. R., Bernhofer, C., … Weidinger, T. (2007). The energy balance experiment EBEX-2000. part i: Overview and energy balance. *Boundary-Layer Meteorology, 123*(1), 1–28. https://doi.org/10.1007/s10546-007-9161-1

Pardyjak, E., Calaf, M., Hultmark, M., Higgins, C. W., Iungo, G., … Kokmanian, K. (2018). An overview of the Idealized Planar Array experiment for Quantifying Surface heterogeneity (IPAQS) in the atmospheric surface layer experiment. – In: AGU Fall Meeting Abstracts, volume 2018, A52D–02.

Raasch, S., & Schröter, M. (2001). Palm – a large-eddy simulation model performing on massively parallel computers. *Meteorologische Zeitschrift (Berlin), 10*(5), 363–372. https://doi.org/10.1127/0941-2948/2001/0010-0363

Raupach, M. R., & Shaw, R. H. (1982). Averaging procedures for flow within vegetation canopies. *Boundary-Layer Meteorology, 22*(1), 79–90. https://doi.org/10.1007/BF00128057

Saiki, E. M., Moeng, C. H., & Sullivan, P. P. (2000). Large-eddy simulation of the stably stratified planetary boundary layer. *Boundary-Layer Meteorology, 95*(1), 1–30. https://doi.org/10.1023/A:1002428223156

Steinfeld, G., Letzel, M. O., Raasch, S., Kanda, M., & Inagaki, A. (2007). Spatial representativeness of single tower measurements and the imbalance problem with eddy-covariance fluxes: Results of a large-eddy simulation study. *Boundary-Layer Meteorology, 123*(1), 77–98. https://doi.org/10.1007/s10546-006-9133-x

Stiperski, I., & Calaf, M. (2023). Generalizing monin-obukhov similarity theory (1954) for complex atmospheric turbulence. *Physical Review Letters, 130*(12), 124001. https://doi.org/10.1103/PhysRevLett.130.124001

Stoy, P. C., Mauder, M., Foken, T., Marcolla, B., Boegh, E., Ibrom, A., … Van Gorsel, E. (2013). A data-driven analysis of energy balance closure across FLUXNET research sites: The role of landscape scale heterogeneity. *Agricultural and Forest Meteorology, 171–172*, 137–152. https://doi.org/10.1016/j.agrformet.2012.11.004

Sühring, M., & Raasch, S. (2013). Heterogeneity-induced heat-flux patterns in the convective boundary layer: Can they be detected from observations and is there a blending height? – a large-eddy simulation study for the LITFASS-2003 experiment. *Boundary-*

Layer Meteorology, 148(2), 309–331. https://doi.org/10.1007/s10546-013-9822-1

Taylor, G. I. (1938). The spectrum of turbulence. *Proceedings of the Royal Society of London. Series A, Mathematical and Physical Sciences, 164*(919), 476–490. https://doi.org/10.1098/rspa.1938.0032

Uhlenbrock, J., Raasch, S., Hennemuth, B, Zittel, P, Meijninger, W. M. L. (2004). Effects of land surface heterogeneities on the boundary layer structure and turbulence during LITFASS-2003: large-eddy simulations in comparison with turbulence measurements. – In: 6th Symposium on boundary layers and turbulence. American Meteorological Society, Portland (Maine), paper 9,3.

Wanner, L., de Roo, F., Sühring, M., & Mauder, M. (2022). How does the choice of the lower boundary conditions in large-eddy simulations affect the development of dispersive fluxes near the surface? – *Boundary-Layer Meteorology, 182*(1), 1–27. https://doi.org/10.1007/s10546-021-00649-7

Wanner, L., Jung, M., Paleri, S., Butterworth, B. J., Desai, A. R., Sühring, M., & Mauder, M. (2024). Towards energy-balance closure with a model of dispersive heat fluxes. *Boundary-Layer Meteorology, 190*(5), 25. https://doi.org/10.1007/s10546-024-00868-8

Wicker, L. J., & Skamarock, W. C. (2002). Time-splitting methods for elastic models using forward time schemes. *Monthly Weather Review, 130*(8), 2088–2097. https://doi.org/10.1175/1520-0493(2002)130<2088:TSMFEM>2.0.CO;2

Williamson, J. H. (1980). Low-storage runge-kutta schemes. *Journal of Computational Physics, 35*(1), 48–56. https://doi.org/10.1016/0021-9991(80)90033-9

Wilson, K., Goldstein, A., Falge, E., Aubinet, M., Baldocchi, D., Berbigier, P., … Verma, S. (2002). Energy balance closure at FLUXNET sites. *Agricultural and Forest Meteorology, 113*(1-4), 223–243. https://doi.org/10.1016/S0168-1923(02)00109-0

Zhou, Y., Sühring, M., & Li, X. (2023). Evaluation of energy balance closure adjustment and imbalance prediction methods in the convective boundary layer – a large eddy simulation study. *Agricultural and Forest Meteorology, 333*, 109382. https://doi.org/10.1016/j.agrformet.2023.109382

Manuscript received: November 4, 2023
Revisions requested: December 21, 2023
Revised version received: April 29, 2024
Manuscript accepted: May 29, 2024